



# Observation of the Tailward Electron Flows Commonly Detected at the Flow Boundary of the Earthward Ion Bursty Bulk Flows in the Magnetotail

Mao Zhang<sup>1,2</sup> , Rongsheng Wang<sup>1,2</sup>, Quanming Lu<sup>1,2</sup> , and Shui Wang<sup>1,2</sup>

<sup>1</sup> CAS Key Laboratory of Geospace Environment, Department of Geophysics and Planetary Science, University of Science and Technology of China, Hefei 230026, People's Republic of China; [rswan@ustc.edu.cn](mailto:rswan@ustc.edu.cn)

<sup>2</sup> CAS Center for Excellence in Comparative Planetology, People's Republic of China

Received 2019 September 3; revised 2020 January 16; accepted 2020 February 2; published 2020 March 17

## Abstract

Using measurements of the *Magnetospheric Multiscale* mission in the magnetotail from  $-24$  to  $-15R_E$ , we identified 40 ion Bursty Bulk Flow events (BBFs) and investigated the electron behaviors during these BBFs. The ion flows peaked near the center of the plasma sheet and had a sharp flow boundary. The electron-flow profile is distinct from the ion flows of the BBFs. Inside the BBFs, the strongest Earthward electron flows are observed in the ion flow boundary, away from the current sheet center. Farther away from the peak of the Earthward electron flows, the tailward electron flows are observed in the edges of the ion flows, are mainly field-aligned with low energy, and are stronger than the Earthward flows. It seems that the tailward low-energy electrons are energized at some places tailward of the spacecraft and then ejected Earthward, consistent with the magnetic reconnection scenario in the magnetotail. We suggest this has implications for our understanding of astrophysical jets.

*Unified Astronomy Thesaurus concepts:* [Space plasmas \(1544\)](#); [Interplanetary particle acceleration \(826\)](#); [Solar magnetic reconnection \(1504\)](#)

## 1. Introduction

Astrophysical jets are ubiquitous throughout the universe. They are observed in many astrophysical contexts, such as the active galactic nuclei and the low-mass young stellar objects within our own galaxy (e.g., Ferrari 1998; Gounveia dal Pino 2005). The jets in widely diverse astrophysical environments display a collimated outflow and are responsible for the transport of mass, momentum, energy, and magnetic flux through the ambient, in either the interstellar or the intergalactic medium. In astrophysical contexts, the jets/outflows are believed to be driven by magnetic fields or rotation via an accretion disk (Ferreira 1997; Ouyed et al. 1997). Numerical studies show the magnetically launched jets can accelerate to only a few times the Alfvén speed (Fendt & Camenzind 1996). These supersonic jets are believed to form a velocity shear at their boundary regions and accelerate particles (Rieger & Duffy 2004). Kelvin–Helmholtz instability has been suggested to be triggered within the jet boundary region, leading to the mixture of jets with ambient material (Bodo et al. 1995, 1998). However, the lack of in situ observation in most astrophysical environments makes it hard to further study the details of such dynamic jets. Utilizing accurate measurements of terrestrial satellites, we can study the fine structures and boundary formation of similar plasma jets in the Earth's magnetosphere, which are known as bursty bulk flows (BBFs). The results can improve our understanding of astrophysical jets.

One kind of plasma jet in the Earth's magnetotail is the BBF, which is frequently observed in the magnetotail and plays a key role in transferring the mass, energy, momentum, and magnetic fluxes in the Earth's magnetosphere (Baumjohann et al. 1990; Angelopoulos et al. 1992, 1994, 1996; Cao et al. 2006, 2013). The BBFs in the inner plasma sheet are generally considered to be the result of magnetic reconnection (Nagai et al. 1998; Øieroset et al. 2000; Shay et al. 2003; Fu et al. 2006; Wang et al. 2012), and the bulk flow speed approaches the local Alfvénic speed (Baumjohann et al. 1990). While propagating

Earthward, the BBFs oscillate back and forth and are diverted at the braking region due to the Earth's dipolar magnetic field (Panov et al. 2010, 2013; Nakamura et al. 2013; Pritchett & Runov 2017). The ion properties in the BBFs, including the ion temperature, distribution, velocity, and density have been extensively studied based on observations of spacecraft such as, *Geotail*, *Cluster*, and *Time History of Events and Macroscale Interactions during Substorms (THEMIS)*; e.g., Nakamura et al. 2004; Cao et al. 2006, 2013; Ma et al. 2009; Zhang et al. 2009).

Much effort has been devoted to electron behaviors in the plasma sheet. The results exhibit that the electron dynamics is dramatically different from that of the ions. The electron pitch angle distribution shows that perpendicular electrons dominated at the center of the plasma sheet and became bidirectional as the plasma beta decreased (Walsh et al. 2011, 2013). Furthermore, a net cold electron flow in the field-aligned direction was observed and seemed to originate from the ionosphere rather than the magnetosheath (Walsh et al. 2013). The energy distribution of the anisotropic electron population varied with the downtail distance and along the dawn–dusk direction, and was modified by the  $B_z$  component in the Geocentric Solar Magnetospheric (GSM) coordinate (Artemyev et al. 2014). Different from ion measurements, electron bulk flows can only be accurately measured recently by the *Magnetospheric Multiscale (MMS)* mission. The initial results show that the electron bulk flows are much stronger than the ion bulk flows in the vicinity of the electron diffusion region (EDR), even in the region far away from the EDR (e.g., Torbert et al. 2018; Yu et al. 2019).

However, due to insufficient measurements of electron motions by previous satellites, the electron bulk flows associated with the BBFs have not been thoroughly studied. In this letter, we try to study the average properties of the electron bulk flows across the BBFs based on the *MMS* unprecedentedly high time-resolution electron measurements. By analyzing all of the BBF cases from May to 2017 August,

**Table 1**  
Selected Intervals

N	Date <sup>i</sup>	UT <sup>ii</sup>	Position <sup>iii</sup> , $R_E$	LA <sup>iv</sup> (km s <sup>-1</sup> )	N	Date <sup>i</sup>	UT <sup>ii</sup>	Position <sup>iii</sup> , $R_E$	LA <sup>iv</sup> (km s <sup>-1</sup> )
1	0605	1335–1337	–20.7, 8.5, 3.5	669	21	0706	2236–2241	–24.6, –1.5, 5.2	742
2	0614	0551–0554	–22.8, –8.0, –4.3	723	22	0709	1038–1050	–24.1, 3.0, 3.9	977
3	0614	0647–0655	–22.9, –8.1, –4.7	826	23	0717	1458–1501	–21.9, 6.8, 2.3	755
4	0617	1039–1046	–22.6, –8.2, 6.6	1128	24	0718	0218–0224	–24.3, 4.0, 5.1	785
5	0619	0357–0359	–16.9, –0.4, 1.6	804	25	0718	0226–0233	–24.3, 4.0, 5.1	733
6	0619	0944–0950	–20.5, –2.0, 3.2	928	26	0718	1843–1847	–20.6, –0.1, 5.7	528
7	0625	0413–0419	–22.4, –1.9, 3.6	806	27	0720	1735–1745	–23.7, 4.3, 4.1	679
8	0706	0054–0057	–17.7, 3.7, 2.4	723	28	0720	1749–1757	–23.8, 6.1, 4.2	771
9	0706	0818–0826	–22.0, 3.1, 3.0	713	29	0720	1918–1921	–24.0, 5.6, 4.7	802
10	0706	0829–0842	–22.1, 3.1, 3.0	521	30	0726	1339–1345	–23.7, 7.9, 2.9	1032
11	0706	0904–0908	–22.3, 3.0, 3.0	530	31	0726	1730–1739	–23.5, 6.4, 4.6	1005
12	0706	1438–1449	–24.0, 1.8, 4.2	880	32	0729	0727–0731	–23.3, 9.2, 2.5	791
13	0706	1546–1558	–24.2, 1.3, 4.5	709	33	0729	1547–1608	–22.8, 7.0, 4.0	808
14	0706	1600–1604	–24.2, 1.2, 4.5	702	34	0807	0834–0839	–20.1, 7.8, 2.8	659
15	0706	1614–1618	–24.3, 1.1, 4.6	774	35	0807	1554–1606	–16.2, 4.1, 3.8	787
16	0706	1625–1638	–24.3, 1.0, 4.6	623	36	0807	1625–1630	–15.8, 3.7, 3.9	760
17	0706	1644–1648	–24.3, 0.9, 4.7	654	37	0807	1632–1637	–15.8, 3.7, 3.9	795
18	0706	1653–1657	–24.3, 0.8, 4.7	672	38	0807	1657–1706	–15.4, 3.4, 4.0	1018
19	0706	1659–1703	–24.3, 0.8, 4.7	674	39	0809	2216–2219	–21.3, 9.7, 4.7	759
20	0706	1946–1951	–24.6, –0.5, 5.1	896	40	0818	1709–1713	–17.3, 8.9, 2.8	1229

**Notes.** (1) Calculate the total pressure in each event by  $P_{\text{tot}} = P_i + B^2/2\mu_0$ ; (2) calculate the lobe magnetic field by  $\overline{B_{\text{tot}}} = B_L^2/2\mu_0$ , where  $\overline{B_{\text{tot}}}$  is the average value of the total pressure; (3) calculate the number density of ions in the inner plasma sheet area by  $\overline{P_{\text{tot}}} = P_i$ ,  $P_i = n_i k T_i$ ; (4) the local Alfvén speed is derived by  $V_A = B_L / \sqrt{\mu_0 \rho_i}$ .

<sup>i</sup> Date format: mmdd of 2017.

<sup>ii</sup> BBF intervals in burst-mode data.

<sup>iii</sup> The position of *MMS* in GSM coordinates during the selected interval.

<sup>iv</sup> The local Alfvén speed in each BBF event.con

we determine the profile of the electron bulk flow velocity, electron density, and electron temperature across the plasma sheet and suggest that this finding has implications for our understanding of astrophysical jets.

## 2. Database and Case Study

In this article, the data from several instruments on board *MMS* were used. The magnetic-field data were obtained from the flux-gate magnetometers instruments with a time resolution of 128 Hz (Torbert et al. 2016). The ion and electron moments were taken from the Fast Plasma Investigation (FPI). The time resolution is 150 ms for ions and 30 ms for electrons (Pollock et al. 2016). Considering that the electrons are moving fast and the speed evolves quickly during the BBFs, we only chose the time interval in burst mode. Furthermore, in order to study the electron flows across the plasma sheet with the BBFs, we only chose the BBF events with complete crossing(s) of the plasma sheet, or at least partial crossing from the center plasma sheet to the flow boundary of the BBFs or vice versa. The criteria used to select the BBF events include (1) the peak value of the plasma beta  $\beta > 2$  to ensure that the spacecraft entered into the plasma sheet, and (2) the maximum value of the ion flows  $V_{ix} > 400 \text{ km s}^{-1}$ . Between 2017 May and August, the *MMS* spacecraft passed through a wide range in the magnetotail  $-24R_E < X < -15R_E$  in the GSM system. In order to avoid the complicated plasma flows at the flank region, the events between  $|Y| < 10 R_E$  are chosen. Then, we obtained the 40 BBF events listed in Table 1.

Figure 1 shows one example of these BBF events observed at  $[-24.3, 0.9, 4.7] R_E$  in GSM coordinates on 2017 July 6. From top to bottom, three components and magnitudes of the magnetic field, parallel and perpendicular temperatures of ions

and electrons, plasma beta, the ion flow velocities, electron velocity vector, parallel and perpendicular electron velocity, and ion and electron energy–time spectra are displayed. During the whole interval of 16:34:40 ~ 16:38:13 UT, *MMS* stayed in the north hemisphere at most times ( $B_x \sim 10 \text{ nT}$ , Figure 1(a)), and crossed the neutral sheet several times at  $\sim 16:36:15 \text{ UT}$ ,  $\sim 16:37:00 \text{ UT}$  and  $\sim 16:37:45 \text{ UT}$ ; the plasma beta was larger than 0.5, except for a short span at the end of the interval (after 16:38 UT, Figure 1(d)). This indicates that the spacecraft was located in the plasma sheet before 16:38 UT. For the whole time interval, the high-speed ion bulk flows were persistently detected, primarily in the  $x$  direction. Sometimes, its speed was as large as  $1000 \text{ km s}^{-1}$ . Overall, the ion and electron temperature were enhanced when ion bulk flows rose (Figures 1(b) and (c)), with a few localized minima. The observation was consistent with the previous observation of the BBFs (Angelopoulos et al. 1992, 1994). Therefore, we concluded that a BBF event was observed during this interval. We have to point out that the FPI instrument cannot completely cover all of the energy range of the ions in the central plasma sheet ( $\beta > 2$  in this event). Thus, the ion bulk flow speed should be underestimated then. However, in the region with rather lower  $\beta (\leq 2)$ , the energy range of the main population is included by the FPI instrument (e.g., 16:34:50–16:35:20 UT, 16:37:20~16:37:40 UT in Figure 1(h)). Thus, in the low  $\beta$  region, the ion moment data are accurate. On the other hand, the electrons can be measured properly by the FPI instrument. Since here we will focus on the electron properties and the boundary region, the underestimation of the ion bulk flows in the central plasma sheet does not alter our results.

Inside this BBF, the high-speed electron flows were simultaneously observed as well. The electron bulk flows were

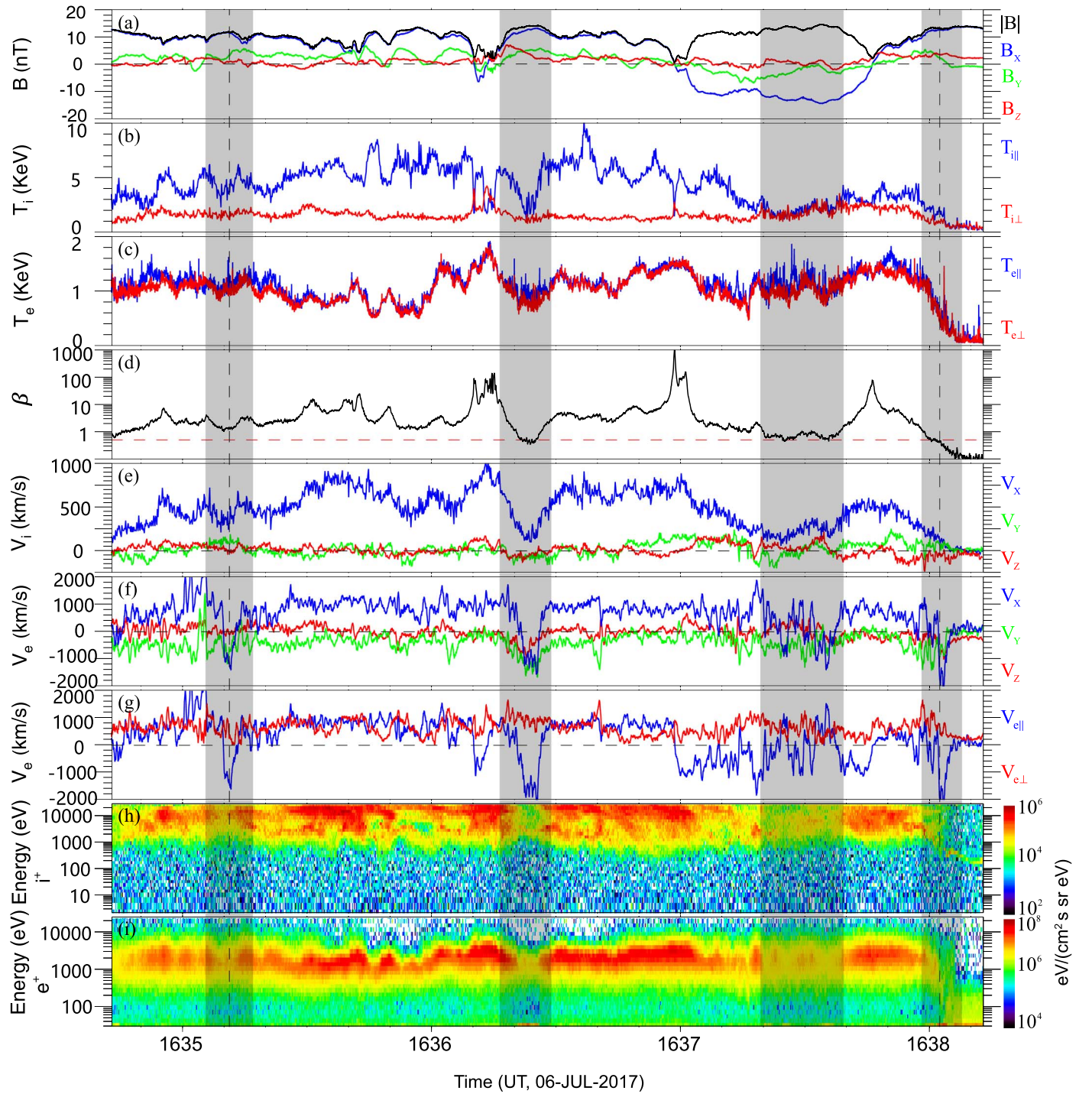


**Figure 1.** Overview of a typical BBF event obtained by *MMS1*. The satellite was located at  $[-24.3, 0.9, 4.7] R_E$  in GSM coordinates. (a) Three components and magnitudes of the magnetic field; (b) and (c) parallel and perpendicular temperatures of ions and electrons; (d) plasma beta; (e) and (f) ion and electron-flow velocities; (g) parallel and perpendicular velocities of electron flow; (h) and (i) energy–time spectrum of ions and electrons. The shadow areas indicate four spells of the tailward electron flows.

basically  $\sim 1000 \text{ km s}^{-1}$ . Although the electron flows primarily moved Earthward like the ion flows, they became tailward occasionally at  $\sim 16:35:12 \text{ UT}$ ,  $\sim 16:36:25 \text{ UT}$ ,  $\sim 16:37:25 \text{ UT}$ , and  $\sim 16:38:04 \text{ UT}$  (Figure 1(f)), as marked by the shadowed areas in Figure 1. Figure 1(g) shows the parallel electron bulk flows (blue trace) and absolute values of the perpendicular electron flows (red trace). The tailward electron flows are primarily the field-aligned ones. Furthermore, the tailward electron flow exactly coincided with depression of the plasma

beta (Figure 1(d)) and ion flow speed (Figure 1(e)), its duration was only about a few seconds. It seems that the tailward electron flows are always detected in the regions with a strong magnetic field, which can be found more clearly from the straight crossing during  $16:37:30\text{--}16:38:10 \text{ UT}$ . In this crossing, *MMS* completely passed through the whole plasma sheet from south to north, and the high-speed ion flows peaked at the center and were bounded by the tailward electron flows at  $\sim 16:37:35 \text{ UT}$  and  $\sim 16:38:03 \text{ UT}$  (Figure 1(f)). The tailward

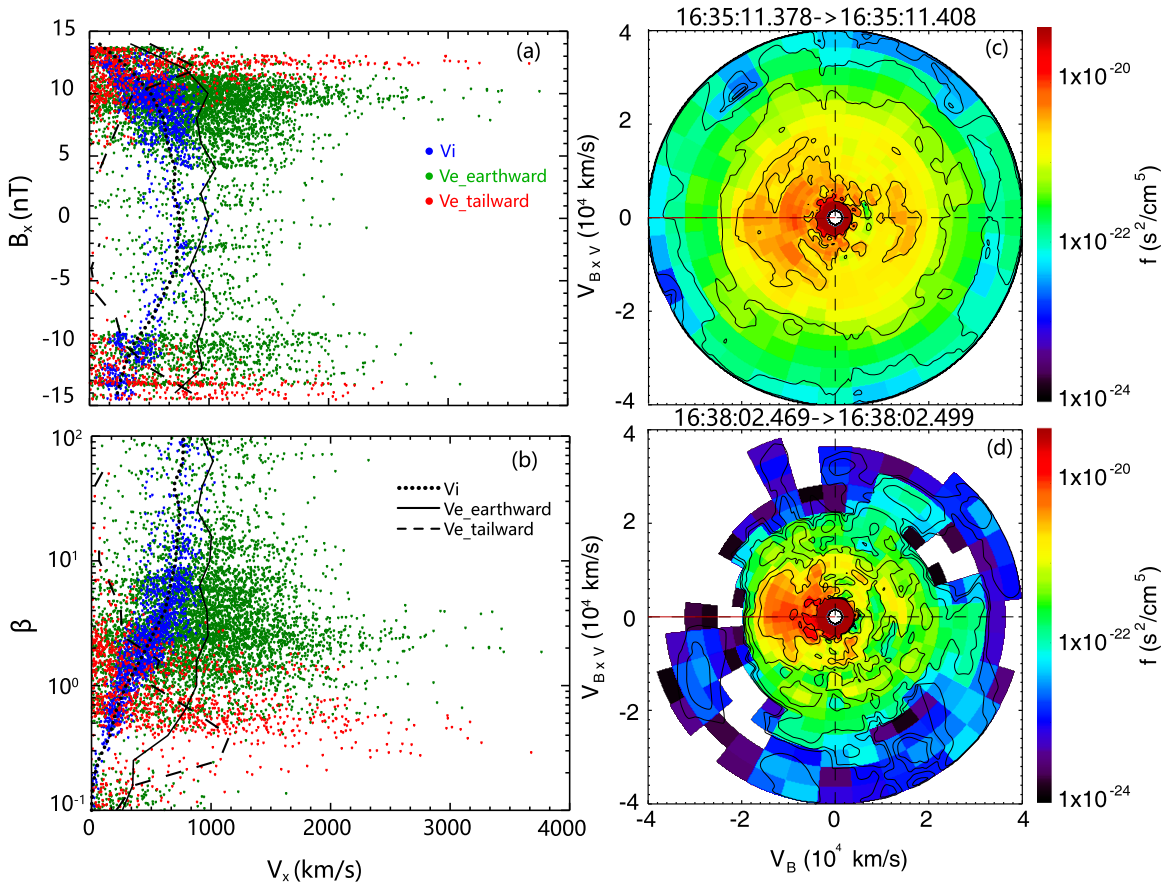


**Figure 2.** (a) Scatter plot and average speed of  $B_x$  vs.  $V_x$ ; (b) scatter plot and average speed of plasma beta vs.  $V_x$ ; (c) and (d) electron distributions during these two intervals of the tailward electron flows. The center time of each electron distribution is marked by the vertical dashed line in Figure 1.  $v_B$  indicates the direction parallel to the magnetic field and  $v_{B \times v}$  indicates the direction perpendicular to the magnetic field.

electron flows only lasted for about 2 s, much shorter than the duration of the ion flows, which lasted for 28 s. Assuming that *MMS* crossed the sheet constantly, then the thickness of the region with the tailward electron flows was only about 6% of the whole plasma sheet.

In order to figure out the profiles of the electron and ion flows across the plasma sheet, the scatter plots between  $B_x$  and ion flows  $V_{ix}$  (blue dots), Earthward electron flow  $V_{ex}$  (green dots), and tailward electron flows (red dots) during 16:34:40–16:38:13 UT are shown in Figure 2(a), and the scatter plots between  $\beta$  and the flows are shown in Figure 2(b). The average speed of ion flows  $V_{ix}$  (dotted line), Earthward electron flows  $V_{ex}$  (solid line), and tailward electron flows (dashed line) are also presented in Figures 2(a) and (b). Because of the different time resolutions of the plasma and magnetic-field data, the magnetic-field data were interpolated to the plasma data. The ion flow speed (blue dots) was the strongest around the central plasma sheet ( $|B_x| < 5$  nT) and gradually decreased away from the center (Figure 2(a)). In Figure 2(b), the ion flow speed reached the maximum value at  $\beta > 10$  and gradually decayed as  $\beta$  declined. The ion flow speed was basically less than  $800 \text{ km s}^{-1}$ . These ion features are consistent with those of previous observations (e.g., Angelopoulos et al. 1992; Wang et al. 2014).

In contrast, the average speed of Earthward electron flows (solid line) was  $\sim 900 \text{ km s}^{-1}$  and substantially stronger than the ion speed. The electron-flow profile across the plasma sheet did not show a feature similar to that of the ions. The high-

speed Earthward electron flows had a wider flow channel than the ion flows. Their speeds remained higher than  $800 \text{ km s}^{-1}$  at  $|B_x| \leq 11$  nT (Figure 2(a)) or  $\beta > 1$  (Figure 2(b)). At the boundary region of ion flows (ion flow shear region), the extremely high-speed ( $> 1500 \text{ km s}^{-1}$ ) Earthward electron flows were detected (green dots) and these data points were centered at  $\beta \sim 3$  or  $|B_x| \sim 10$  nT. These extremely high-speed electron flows suggested the flow disturbances at the boundary region. Another striking feature of the electron flows across the BBFs is the tailward flows (red dots in Figure 2(a)). The tailward flows with significant speed, comparable to the Earthward flows, were almost all observed with a large value of  $|B_x| (> 10 \text{ nT})$  and a low  $\beta (< 2)$ , just the flow boundaries of the ion BBFs (Figure 2(a)), and the speed could exceed  $3000 \text{ km s}^{-1}$ . Moreover, the region with the tailward electron flows was very narrow compared to the width of the BBFs in the normal direction of the plasma sheet.

Based on the observations above, the electron-flow profile was distinct from the ions in this BBF event, which indicates that the electron and ion dynamics are different in the BBFs. The electron and ion frozen-in conditions were checked in this event as well. The results show that the electrons were principally coupled with magnetic fields, while ions were not (not shown). The electrons were properly measured by the FPI instrument, which was the main goal of this study. Therefore, the results on the electron-flow profile across the BBFs is reliable. Given the errors of the ion flow speed, we cannot conclude that the ions must be decoupled from the electrons or

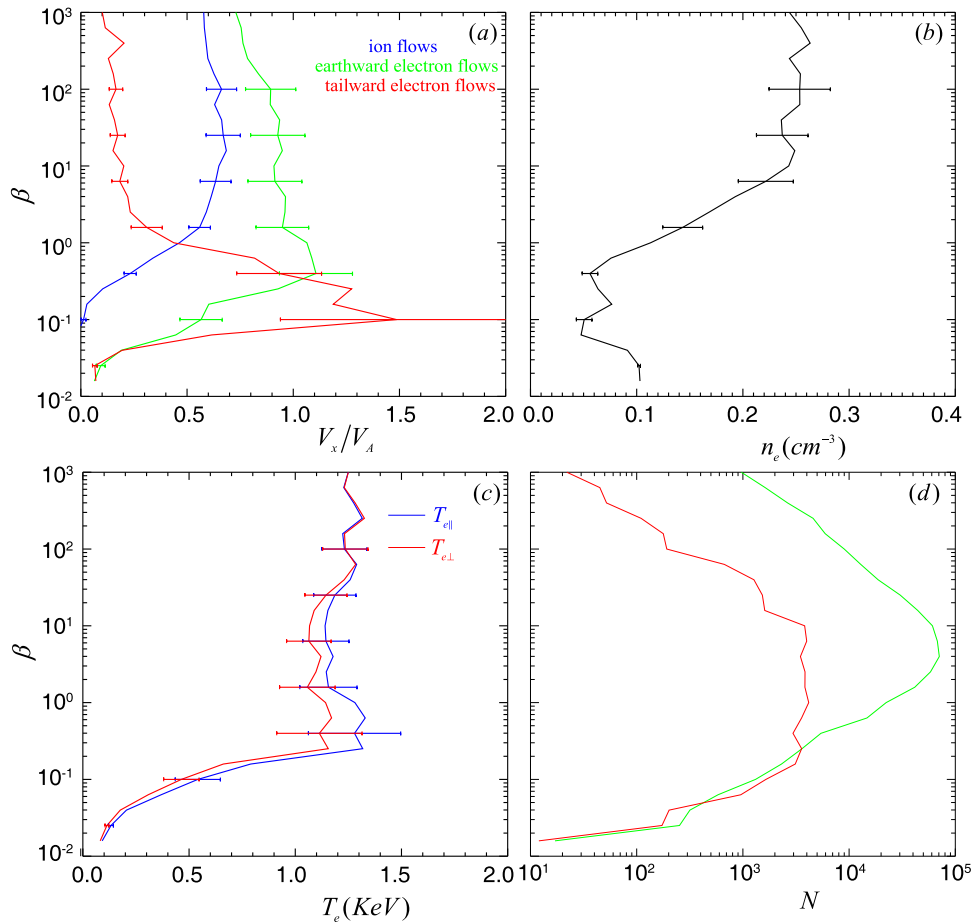


**Figure 3.** Statistical results of 40 BBF intervals. All the plasma properties are averaged in each  $\beta$  bin (a)–(d). (a) Average bulk velocity (normalized with local Alfvén speed) in the  $X_{\text{GSM}}$  direction; (b) number density of electrons; (c) temperature of electrons; (d) number of data points in each  $\beta$  bin. In graph (a), the blue line indicates the ion flow velocity, the green line indicates the Earthward electron-flow velocity, and the red line indicates the tailward electron-flow velocity. The calculation of the local Alfvén speed can be found in Table 1. The error bars were equivalent to one-fifth of the standard deviations.

the ion bulk flows must be smaller than the electrons. But, in the region with low beta ( $\beta \leq 2$ ) where the ion bulk flows are basically reliable, we still found that the electron-flow speed was, on average, much higher than that of the ions. This indicates that the flow difference between ions and electrons is real in this event.

Figures 2(c) and (d) display the electron distribution functions in the plane of  $v_B - v_{B \times V}$  during the tailward electron flows, where  $v_B$  means the velocity along the magnetic field and  $v_{B \times V}$  denotes the direction  $B \times V_e$  perpendicular to the magnetic field, and the sampled time is marked by the vertical dashed line in Figure 1. In Figure 2(c), the bidirectional electron distribution can be found, and the fluxes in the direction antiparallel to the magnetic field are larger than that in the parallel direction. As a result, net electron flows in the antiparallel direction were observed and the energy range of the electrons was mainly from 30 eV ( $3000 \text{ km s}^{-1}$ ) to 1.1 keV ( $20,000 \text{ km s}^{-1}$ ). Figure 2(d) represents the electron distribution when the spacecraft got into the plasma sheet boundary layer ( $\beta < 0.3$ ) (abbreviated as PSBL). The electron fluxes are dramatically depressed but the beam electron distribution antiparallel to the magnetic field is very clear, and the energy range of the electron beam is the same as that in Figure 2(c). Therefore, this tailward electron flow connects to the field-aligned current in the PSBL (Nakamura et al. 2016; Chen et al. 2019). Within the tailward electron flows, the electron

temperature shows that the parallel temperature (blue trace) is slightly higher than the perpendicular temperature (Figure 1(c), red trace), with some  $T_{e\parallel}$  and  $T_{e\perp}$  spikes that were common for all the BBFs.

According to the observations above, the tailward electron flows were observed at the north and south flow boundaries of the BBFs. The tailward electron flows were primarily parallel or antiparallel to the magnetic field, their energies were mainly less than 1 keV, and their bulk flow speed was as high as the Earthward electron flows. It appears that the tailward electron flows were colder than the Earthward electron flows and some of the tailward electron flows were directly connecting with the field-aligned current in the PSBL. In order to figure out whether or not these electron characteristics are common during the BBFs, a statistical study of the 40 BBF events is presented in the next section.

### 3. Statistical Results of the BBFs

Figure 3 shows the results of the statistical analysis of all 40 BBF events. The plasma properties were averaged in the  $\beta$  bin (panels (a)–(d)).  $\beta$  was split into 25 equally sized bins in a logarithmic frame, the center of the lowest bin corresponding to  $\log_{10}(\beta) = -2$  and the highest to  $\log_{10}(\beta) = 3$ . When calculating the average plasma properties, we assigned the same weight to all data points. One may question if the long-duration event can influence the average value. However, it

should be emphasized that the long-duration event also covers a broader range in the plasma sheet. Thus, this method is acceptable in principle.

Figures 3(a)–(d) show the profile of the ion and electron bulk flow speed along the  $X_{\text{GSM}}$  direction, the electron number density, electron temperature, and the number of data points in each  $\beta$  bin. The electron bulk flow speed was normalized with the local Alfvén speed. The error bar was also given and the details of the calculation method can be found in Baumjohann et al. (1989). Assuming the pressure balance across each crossing of the plasma sheet ( $P_{\text{total}} = P_i + B_L^2/2\mu_o = \text{const}$ ), we can get the magnetic field in the lobe region ( $B_L = \sqrt{2\mu_o P_{\text{total}}}$ ) and the plasma density in the neutral sheet of the plasma sheet ( $n_i = P_{\text{total}}/kT_i$ ), where  $\mu_o$  and  $k$  denote permeability of the vacuum and Boltzmann constant, respectively. The Alfvén speed is obtained from the equation  $V_A = B_L/\sqrt{\mu_o n_i m_i}$ . Since the spacecraft separation was small and the data from all four satellites are more or less the same, we only use the data from *MMS1*. Figure 3(a) displays the measured ion moment data (blue solid curve), the measured Earthward electron flow (green solid curve), and the measured tailward electron flow (red solid curve) in the  $X_{\text{GSM}}$  direction. It can be seen clearly that the Earthward ion flow velocity was the strongest ( $\sim 0.7V_A$ ) in the central plasma sheet ( $\beta \geq 10$ ). In the region with the low beta ( $0.1 < \beta < 2$ ), the Earthward ion flows sharply decreased from  $\sim 0.5V_A$  to  $\sim 0$ . This narrow layer with intense ion shear was defined as the flow boundary of the BBFs.

The Earthward electron flows show a different pattern from the Earthward ion flows. In the central plasma sheet ( $\beta \geq 10$ ), the electron bulk flows were as large as  $\sim 0.95V_A$ , while in the flow boundary of the BBFs ( $0.1 < \beta < 2$ ), the Earthward electron flow had a maximum value up to  $1.1V_A$  at  $\beta = 0.5$  and then sharply decreased as  $\beta$  declined. The tailward electron flows were very weak ( $< 0.2V_A$ ) in the region with a high  $\beta$  ( $> 2$ ), began to grow from  $\beta \sim 1$  as  $\beta$  declined, and peaked at  $\beta \sim 0.1$  farther away from the center of the plasma sheet than the peak of the Earthward electron flows. The peak value of the tailward electron flows was up to  $1.4V_A$ , which is higher than the Earthward electron flows. Furthermore, the strong tailward electron flows were basically observed in the very narrow region corresponding to the outer edges ( $\beta \leq 0.2$ ) of the BBFs, which is consistent with the case study.

Figure 3(d) shows the number of data points in each  $\beta$  bin. In the high  $\beta$  area ( $\beta > 2$ ), the data points of the Earthward electron flows were more than one order of magnitude higher than those of the tailward electron flow. This means that the flows were primarily Earthward in the high  $\beta$  region. The tailward electron flows within the BBFs were very weak ( $< 0.2V_A$ ) and attributed to the intermittent fluctuations of the electron flow. In the flow edges of the BBFs ( $\beta \leq 0.2$ ), however, the data points of the tailward electron flows were comparable to or even higher than those of the Earthward electron flows. This indicates that the tailward electron flows in that region were reliable, rather than caused by the flow fluctuations.

The electron number density versus  $\beta$  is depicted in Figure 3(b). The density kept a high level ( $0.23 \text{ cm}^{-3}$ ) as  $\beta > 2$  and decreased to  $0.06 \text{ cm}^{-3}$ , while  $\beta$  was less than 0.6. The electron temperature shows a similar variation. It was about 1.2 keV within the BBFs and sharply decreased to  $\sim 100 \text{ eV}$  in the region  $\beta < 0.25$  (Figure 3(c)). Thus, the

tailward electron flows were observed in the flow boundary of the BBFs with a low density and low temperature. Moreover, a noteworthy feature in Figure 3(c) is the electron temperature anisotropy  $T_{e\parallel}/T_{e\perp} > 1$  in the region  $0.25 < \beta < 55$ , which is in accordance with the results of Walsh et al. (2013).

#### 4. Discussion and Summary

Based on the *MMS* measurements in the terrestrial magnetotail from  $-15$  to  $-24 R_E$ , we investigated one typical BBF event and performed statistical analysis of 40 BBF events, and found that the ion flows peaked around the central plasma sheet and gradually decreased away from the center, consistent with previous observation and simulation results (e.g., Kim et al. 2010; Birn et al. 2011; Wiltberger et al. 2015; Zhang et al. 2015); the flows then were sharply depressed in the region of  $0.1 < \beta < 2$ . This intense flow shear layer is defined as the flow boundary of BBFs. The electron flows exhibit different features with respect to the ion flows. Inside the BBFs, the electron flows fluctuate largely, even changing direction sometimes around the center of the plasma sheet (red dots at  $\beta > 10$  or  $|B_x| < 5 \text{ nT}$  in Figures 2(a) and (b)). In contrast to the ion flows, on average, Earthward electron flows had a maximum value ( $\sim 1.1 V_A$ ) at  $\beta \approx 0.4$ , gradually decreasing as  $\beta$  increases, and sharply depressing as  $\beta$  falls from 0.3 to 0.02 (Figure 3(a)). In the sharp depression region of the Earthward electron flows, i.e., the edges of the Earthward electron flows, intense tailward electron flows up to  $1.5 V_A$  are observed. On average, the tailward electron flows are primarily field-aligned, and related to the low density. Additionally, the highest speed for the tailward electron flows is stronger than that for the Earthward flows. The intense tailward electron flows are confined to a narrow region with respect to the Earthward electron flows that is distributed over a much larger range from  $\beta \approx 0.05$  up to 1000.

According to observations, the BBF channel is located in the central plasma sheet with a sharp flow boundary as  $0.1 < \beta < 2$ . There are no tailward ion flows observed across the channel. On the contrary, the electron flows show a distinct profile across the plasma sheet. The Earthward electron flows are basically stronger than the ions and peaked in the flow boundary of the BBFs, differing from ion flows peaking around the center. Moreover, the tailward electron bulk flows were detected in the flow edges of the BBFs, farther away from the middle plan of the plasma sheet than the peak of the Earthward electron flows.

The electron temperature shows that the electrons tend to be isotropic in the region with a large  $\beta$  ( $> 60$ ) and are characterized by the field-aligned distribution as  $\beta < 55$  (Figure 3(c)), basically consistent with previous measurements (Walsh et al. 2011, 2013). The evolution of such distributions is believed to take place via nonadiabatic pitch angle scattering as the electrons traverse the current sheet (e.g., Sergeev et al. 1983; Walsh et al. 2011). The field-aligned electron flows with low energy ( $< 1 \text{ keV}$ ) have been observed in the plasma sheet boundary layer (with low  $\beta$ ) and are suggested to have originated from the ionosphere (Walsh et al. 2013). These field-aligned electron flows interact with the current sheet in the magnetotail.

Magnetic reconnection frequently happens in the near-Earth tail from  $-15 R_E$  to  $-25 R_E$ , based on the previous spacecraft observations (Sergeev et al. 1995; Miyashita et al. 2003; Machida et al. 2009; Wang et al. 2010b). The observed BBF

events are all included in this region. Previously, it was widely accepted that the ions and the electrons are ejected together away from the reconnection site, leading to the formation of the BBFs in the plasma sheet. It was unexpected that the electron-flow profiles across the BBFs are distinct from the ions. Particularly, the peak value of the electron Earthward flows is away from the center of the plasma sheet and the tailward electron flows are observed at the flow boundary of the BBFs. It remains an open question why the ion and electron flows have such a distinction. Considering the ions and the electrons are ejected Earthward inside the BBFs, it looks like that the tailward electron flows in the boundary of the BBFs are moving toward the source region of the BBFs to compensate for the loss of the plasma therein. However, no tailward ion flows are observed at the boundaries.

The kind of electron flows associated with BBFs are very similar to reconnection outflows (Øieroset et al. 2001; Nagai et al. 2003; Asano et al. 2004; Nakamura et al. 2006; Lu et al. 2010; Wang et al. 2010a; Shay et al. 2011; Huang et al. 2014a, 2014b). In the outflow regions of the magnetic reconnection, the inflowing electron beams are always observed in the separatrix regions, and are tailward in the Earthward direction of the reconnection site, and field-aligned (Nagai et al. 2001; Vaivads et al. 2004; Wang et al. 2010a). Furthermore, the inflowing electrons generally have low energy, are energized at the reconnection diffusion region, and then ejected away from the diffusion region. All of these features are consistent with our observations. Thus, the observed tailward electron flows associated with the BBFs are attributed to the reconnection inflowing electron in the separatrix region. In addition to the profile of the electron flow, the electron temperature anisotropy is also consistent with that in the separatrix region (Pritchett 2010). Additionally, the extremely low electron density is in accordance with the density cavity in the separatrix region (e.g., Mozer et al. 2002; Andre et al. 2004; Wang et al. 2012; Yu et al. 2019).

BBFs have been regarded as a product of magnetic reconnection in the magnetotail. As reconnection proceeds, high-speed ion flows are repeatedly produced and form the observed BBFs. These BBFs transfer mass, magnetic fluxes, and energy from the mid-tail to the near-Earth tail, and then trigger the global disturbance, i.e., a substorm. However, once the BBFs are created, they should disconnect with the reconnection site as they propagate Earthward. There is no reason that the inflowing electron beams are ejected away with the BBFs during magnetic reconnection. One explanation for these tailward electrons is that all 40 BBFs are experiencing ongoing reconnection. Then, the tailward electron flows could be observed as long as the spacecraft detected the ion outflow. If so, the boundary process of BBFs would be modulated by the separatrix dynamics and the observed flow fluctuations could be attributed to these dynamics, such as kinetic Alfvén waves (Shay et al. 2011; Lapenta et al. 2013). This also implies that the reconnection-outflow region can extend very far from the reconnection X-line, at least a few Earth radii (e.g., Wang et al. 2012). The extension of the reconnection structure has been predicted in simulations (e.g., Lapenta et al. 2013). In the dayside magnetopause, the electron-scale currents at the boundary of reconnection exhaust are also observed very far from the X-line (about  $\sim 70$  ion skin depths downstream of the X-line) (Phan et al. 2016). This result is consistent with our conjecture. The long extension of the BBFs in the Sun-earth

direction indicates that the BBFs are analogous to the astrophysical jets, at least in terms of shape. If the formation mechanism(s) are similar, there should be rich microphysics along the flow boundary of the astrophysics jets that should be paid much more attention in the future.

Another possibility is that tailward electron flows are a common feature for BBFs. In previous observations, the bidirectional field-aligned electrons were observed in the plasma sheet boundary layer. Once the reconnection proceeded to the plasma sheet boundary layer, the field-aligned electrons diverged at the reconnection site toward the dawn–dusk direction and then the bidirectional field-aligned electron distribution was replaced by the net tailward electron flows in the boundary layer. Thus, the tailward electron flows were always observed Earthward of the X-line in the boundary of the BBFs. As a result, the cold ionospheric electrons were continuously conveyed into the plasma sheet, thus these cold electrons would be energized by magnetic reconnection. The tailward electron flows were observed at the flow boundaries of BBFs and were predominantly parallel or antiparallel to the magnetic field. Namely, these tailward electron flows generated the short-lived field-aligned currents. Small-scale field-aligned currents near the plasma sheet boundary layer have been reported previously (e.g., Nakamura et al. 2016; Artemyev et al. 2018; Chen et al. 2019) and been suggested originate from magnetotail reconnection. The statistical work here further supports this conclusion.

Even though the reconnection scenario can explain all of the observations, there are some other potential mechanisms, such as interchange instability (Pontius & Wolf 1990; Chen & Wolf 1993), and highly curved magnetic field (Liu 2001), that account for the formation of BBFs. However, these two theories were both conducted in the MHD-frame and thus cannot explain the distinct behavior of electrons and ions in the flow boundary region of BBFs, unless other smaller-scale processes were involved. Examining the data around the selected intervals, we confirmed two reconnecting events reported by Yu et al. (2019) and Wang et al. (2019), which supports our explanation of the reconnection scenario.

In summary, the electron behaviors inside the BBFs are investigated in this article. In the plasma sheet, the Earthward electron-flow speed achieves the maximum value, away from the plasma sheet center, in the sharp flow boundaries of the BBFs. In the region farther away from the middle plane than the Earthward flow peaks, the strong tailward electron flows are observed, mainly field-aligned, and with low energy. The features of the electron-flow profile in the BBFs are in good agreement with the reconnection scenario.

All the *MMS* data used in this work are available at the *MMS* data center (<https://lasp.colorado.edu/mms/sdc/>). This work is supported by the National Science Foundation of China (NSFC) grants (41674143, 41474126, 41331067, and 41421063), the National Basic Research Program of China (2013CBA01503), and the B-type Strategic Priority Program of the Chinese Academy of Sciences, grant No. XDB41000000.

#### ORCID iDs

Mao Zhang  <https://orcid.org/0000-0002-0528-8993>  
 Quanming Lu  <https://orcid.org/0000-0003-3041-2682>

## References

- Andre, M., Vaivads, A., Buchert, S. C., et al. 2004, *GeoRL*, **31**, L03803
- Angelopoulos, V., Baumjohann, W., Kennel, C. F., et al. 1992, *JGR*, **97**, 4027
- Angelopoulos, V., Coroniti, F. V., Kennel, C. F., et al. 1996, *JGR*, **101**, 4967
- Angelopoulos, V., Kennel, C. F., Coroniti, F. V., et al. 1994, *JGR*, **99**, 21257
- Artemyev, A. V., Pritchett, P. L., Angelopoulos, V., et al. 2018, *GeoRL*, **45**, 5836
- Artemyev, A. V., Walsh, A. P., Petrukovich, A. A., et al. 2014, *JGRA*, **119**, 7214
- Asano, Y., Mukai, T., Hoshino, M., et al. 2004, *JGRA*, **109**, A02212
- Baumjohann, W., Paschmann, G., & Cattell, C. A. 1989, *JGR*, **94**, 6597
- Baumjohann, W., Paschmann, G., & Luhr, H. 1990, *JGR*, **95**, 3801
- Birn, J., Nakamura, R., Panov, E. V., & Hesse, M. 2011, *JGRA*, **116**, A01210
- Bodo, G., Massaglia, S., Rossi, P., et al. 1995, *A&A*, **303**, 281
- Bodo, G., Rossi, P., Massaglia, S., et al. 1998, *A&A*, **333**, 1117
- Cao, J. B., Ma, Y. D., Parks, G., et al. 2006, *JGRA*, **111**, A04206
- Cao, J. B., Ma, Y. D., Parks, G., et al. 2013, *JGRA*, **118**, 313
- Chen, C. X., & Wolf, R. A. 1993, *JGR*, **98**, 21409
- Chen, Y., Wu, M., Wang, G., et al. 2019, *JGRA*, **124**, 2873
- Fendt, C., & Camenzind, M. 1996, *A&A*, **313**, 591
- Ferrari, A. 1998, *ARA&A*, **36**, 539
- Ferreira, J. 1997, *A&A*, **319**, 340
- Fu, X. R., Lu, Q. M., & Wang, S. 2006, *PhPI*, **13**, 012309
- Gounveia dal Pino, E. M. 2005, *AdSpR*, **35**, 908
- Huang, C., Lu, Q., Lu, S., et al. 2014a, *JGRA*, **119**, 798
- Huang, C., Lu, Q., Wang, P., et al. 2014b, *JGRA*, **119**, 6445
- Kim, H., Lee, D., Ohtani, S., et al. 2010, *JGRA*, **115**, A12229
- Lapenta, G., Goldman, M., Newman, D., & Markidis, S. 2013, *PhPI*, **20**, 102113
- Liu, W. W. 2001, *JGR*, **106**, 289
- Lu, Q., Huang, C., Xie, J., et al. 2010, *JGRA*, **115**, A11208
- Ma, Y. D., Cao, J. B., Nakamura, R., et al. 2009, *JGR*, **114**, A07215
- Machida, S., Miyashita, Y., Ieda, A., et al. 2009, *AnGeo*, **27**, 1035
- Miyashita, Y., Machida, S., Liou, K., et al. 2003, *JGRA*, **108**, 1022
- Mozer, F. S., Bale, S. D., & Phan, T. D. 2002, *PhRvL*, **89**, 015002
- Nagai, T., Fujimoto, M., Saito, Y., et al. 1998, *JGR*, **103**, 4419
- Nagai, T., Shinohara, I., Fujimoto, M., et al. 2001, *JGR*, **106**, 25929
- Nagai, T., Shinohara, I., Fujimoto, M., et al. 2003, *JGRA*, **108**, 1357
- Nakamura, R., Baumjohann, W., Asano, Y., et al. 2006, *JGRA*, **111**, A11206
- Nakamura, R., Baumjohann, W., Mouikis, C., et al. 2004, *GeoRL*, **31**, L09804
- Nakamura, R., Baumjohann, W., Panov, E., et al. 2013, *JGRA*, **118**, 2055
- Nakamura, R., Sergeev, V. A., Baumjohann, W., et al. 2016, *GeoRL*, **43**, 4841
- Øieroset, M., Phan, T. D., Fujimoto, M., et al. 2001, *Natur*, **412**, 414
- Øieroset, M., Phan, T. D., Lin, R. P., & Sonnerup, B. U. Ö 2000, *JGR*, **105**, 25247
- Ouyed, R., Pudritz, R. E., & Stone, J. M. 1997, *Natur*, **385**, 409
- Panov, E. V., Kubyshkina, M. V., Nakamura, R., et al. 2013, *GeoRL*, **40**, 2505
- Panov, E. V., Nakamura, R., Baumjohann, W., et al. 2010, *GeoRL*, **37**, L08103
- Phan, T. D., Eastwood, J. P., Cassak, P. A., et al. 2016, *GeoRL*, **43**, 6060
- Pollock, C., Moore, T., Jacques, A., et al. 2016, *SSRv*, **199**, 331
- Pontius, D. H., & Wolf, R. A. 1990, *GeoRL*, **19**, 49
- Pritchett, P. L. 2010, *JGRA*, **115**, A10208
- Pritchett, P. L., & Runov, A. 2017, *JGRA*, **122**, 3183
- Rieger, F. M., & Duffy, P. 2004, *ApJ*, **617**, 155
- Sergeev, V. A., Angelopoulos, V., Mitchell, D. G., & Russell, C. T. 1995, *JGR*, **100**, 19121
- Sergeev, V. A., Sazhina, E. M., Tsyganenko, N. A., et al. 1983, *P&SS*, **31**, 1147
- Shay, M. A., Drake, J. F., Eastwood, J. P., & Phan, T. D. 2011, *PhRvL*, **107**, 065001
- Shay, M. A., Drake, J. F., Swisdak, M., et al. 2003, *GeoRL*, **30**, 1345
- Torbert, R. B., Burch, J. L., Phan, T. D., et al. 2018, *Sci*, **362**, 1391
- Torbert, R. B., Russell, C. T., Magnes, W., et al. 2016, *SSRv*, **199**, 105
- Vaivads, A., Khotyaintsev, Y., Andre, M., et al. 2004, *PhRvL*, **93**, 105001
- Walsh, A. P., Fazakerley, A. N., Forsyth, C., et al. 2013, *JGRA*, **118**, 6042
- Walsh, A. P., Owen, J., Fazakerley, A. N., et al. 2011, *GeoRL*, **38**, L06103
- Wang, R., Lu, Q., Du, A., & Wang, S. 2010a, *PhRvL*, **104**, 175003
- Wang, R., Lu, Q. M., Du, A., et al. 2014, *JGRA*, **119**, 9952
- Wang, R., Lu, Q. M., Huang, C., & Wang, S. 2010b, *JGRA*, **115**, A01209
- Wang, R., Nakamura, R., Lu, Q. M., et al. 2012, *JGRA*, **117**, A07223
- Wang, S., Chen, L., Bessho, N., et al. 2019, *GeoRL*, **46**, 5014
- Wiltberger, M., Merkin, V., Lyon, J. G., & Ohtani, S. 2015, *JGRA*, **120**, 4555
- Yu, X., Wang, R., Lu, Q., et al. 2019, *GeoRL*, **46**, 10744
- Zhang, L. Q., Dai, L., Baumjohann, W., et al. 2015, *JGRA*, **120**, 9500
- Zhang, L. Q., Liu, Z. X., Baumjohann, W., et al. 2009, *JGRA*, **114**, A02202